Large-Scale Domain Movements and Hydration Structure Changes in the Active-Site Cleft of Unligated Glutamate Dehydrogenase from *Thermococcus profundus* Studied by Cryogenic X-ray Crystal Structure Analysis and Small-Angle X-ray Scattering[†,‡]

Masayoshi Nakasako,*[,§,||] Testuro Fujisawa,[||] Shin-ichi Adachi,[||] Toshiaki Kudo,*[,⊥] and Sadaharu Higuchi[⊥]

PRESTO, Japan Science and Technology Corporation and The Institute of Molecular and Cellular Biosciences, The University of Tokyo, Yayoi 1-1-1, Bunkyo-ku, Tokyo 113-0032, Japan, and The Harima Institute/SPring-8, RIKEN (The Institute of Physical and Chemical Research), Sayo-gun, Hyogo 679-5143, Japan, and RIKEN (The Institute of Physical and Chemical Research), Hirosawa 2-1, Wako, Saitama 351-0198, Japan

Received October 26, 2000; Revised Manuscript Received January 17, 2001

ABSTRACT: Here we describe the large-scale domain movements and hydration structure changes in the active-site cleft of unligated glutamate dehydrogenase. Glutamate dehydrogenase from *Thermococcus profundus* is composed of six identical subunits of M_r 46K, each with two distinct domains of roughly equal size separated by a large active-site cleft. The enzyme in the unligated state was crystallized so that one hexamer occupied a crystallographic asymmetric unit, and the crystal structure of the hexamer was solved and refined at a resolution of 2.25 Å with a crystallographic *R*-factor of 0.190. In that structure, the six subunits displayed significant conformational variations with respect to the orientations of the two domains. The variation was most likely explained as a hinge-bending motion caused by small changes in the main chain torsion angle of the residue composing a loop connecting the two domains. Small-angle X-ray scattering profiles both at 293 and 338 K suggested that the apparent molecular size of the hexamer was slightly larger in solution than in the crystalline state. These results led us to the conclusion that (i) the spontaneous domain motion was the property of the enzyme in solution, (ii) the domain motion was trapped in the crystallization process through different modes of crystal contacts, and (iii) the magnitude of the motion in solution was greater than that observed in the crystal structure. The present cryogenic diffraction experiment enabled us to identify 1931 hydration water molecules around the hexamer. The hydration structures around the subunits exhibited significant changes in accord with the degree of the domain movement. In particular, the hydration water molecules in the active-site cleft were rearranged markedly through migrations between specific hydration sites in coupling strongly with the domain movement. We discussed the cooperative dynamics between the domain motion and the hydration structure changes in the active site of the enzyme. The present study provides the first example of a visualized hydration structure varying transiently with the dynamic movements of enzymes and may form a new concept of the dynamics of multidomain enzymes in solution.

Proteins fold and work in water, their natural medium. Because water is a complex fluid with unusual physical properties caused by hydrogen bonds (*1*), it has great influences on the dynamics of proteins. Therefore, the interface between water and proteins, the hydration structure, is the subject of much discussion to understand how proteins fold and work in water (*2*).

Hydration structures of proteins have been investigated using various experimental techniques and theoretical simulations, with respect to the amount, the geometry and the influences on the dynamics and stability of proteins (*3*−*8*). Recently, cryogenic X-ray crystallography has provided much information on the static pictures of the hydration structures (*9*, *10*). Perhaps, the most interesting result is that proteins are wrapped by hydration shells stabilized through large-scale networks of hydrogen bonds (*9*). This static picture implies that the dynamic movements in proteins at work require a concerted reorganization of their hydration structures. Although information on the hydration structures is still limited in the static case, snapshots of transiently varying hydration structures around proteins at work are required to describe completely how proteins work in water.

For experimentally visualizing transient hydration structures, good targets are multidomain enzymes exhibiting large-

[†] This work was supported by grants-in-aid from the Ministry of Education, Science, Sports and Culture of Japan and the grants for Biodesign and the SR Structural Biology Research Programs from RIKEN. The SAXS experiment was performed under an approval of the organizing committee of SPring-8 (proposal no. 1999B0056-NL-np).

[‡] The atomic coordinate is deposited to the Protein Data Bank under the accession code of 1EUZ.

* To whom correspondence should be addressed. (M.N.) Phone: (81)-3-5841-8493. Fax: (81)-3-5841-8493. E-mail: nakasako@iam.u-tokyo.ac.jp. (T.K.) Phone: (81)-48-467-9544. Fax: (81)-48-462-4672. E-mail: tkudo@postman.riken.go.jp.

[§] Japan Science and Technology Corporation and The University of Tokyo.

[||] The Harima Institute/SPring-8, RIKEN (The Institute of Physical and Chemical Research).

[⊥] RIKEN (The Institute of Physical and Chemical Research).

10.1021/bi002482x CCC: $20.00
Published on Web 02/15/2001

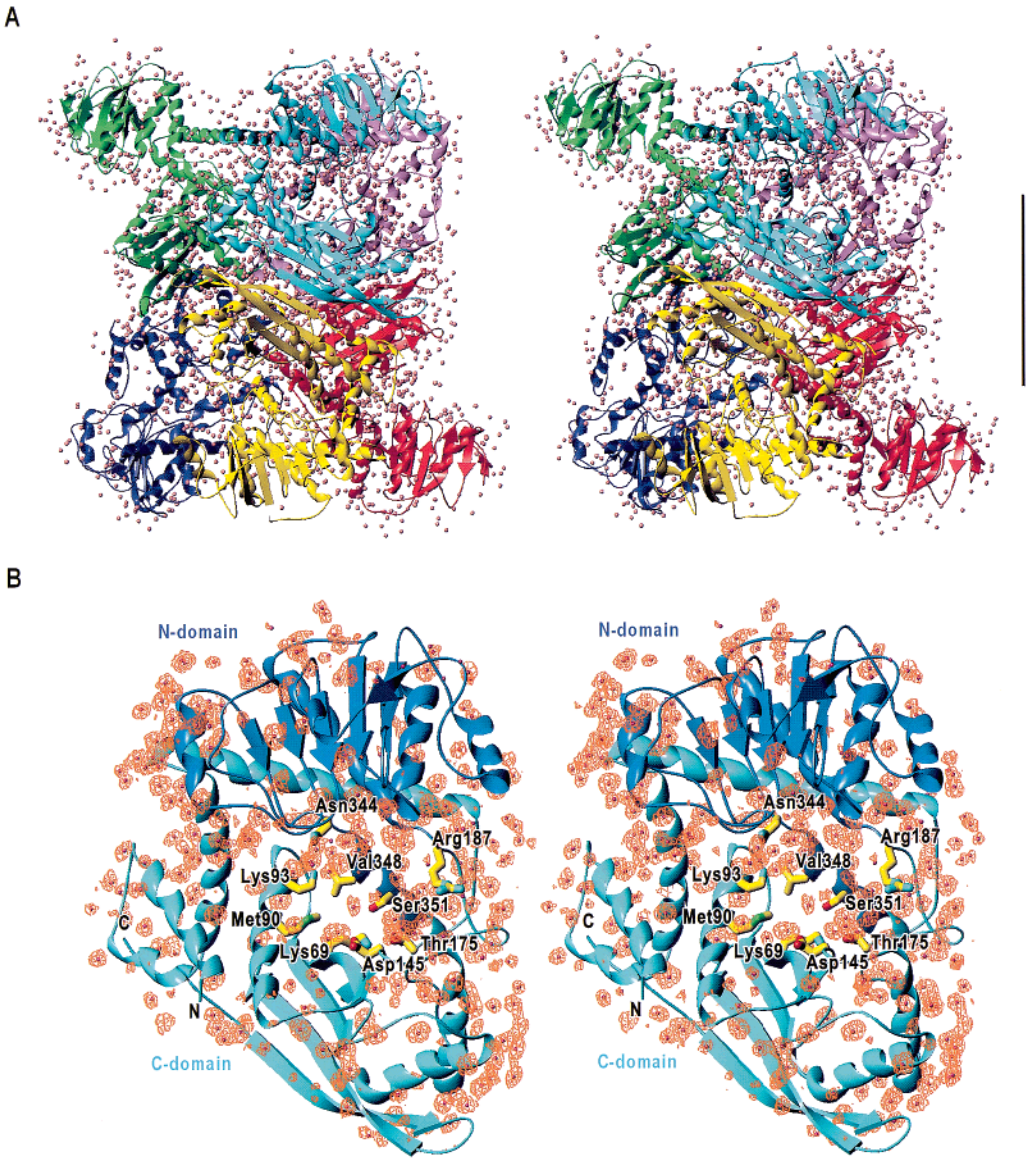

FIGURE 1: (A) Stereoview of hexameric GluDH from *Tp* in a crystallographic asymmetric unit. The six subunits are shown as ribbon models and are distinguished by their colors (subunit1, cyan and blue; subunit2, pink; subunit3, green; subunit4, indigo; subunit5, red; subunit6, yellow). The secondary structures in the ribbon model were defined using the DSSP program (*47*). The colors of C-domain and N-domain are distinguished only in subunit 1. The small spheres indicate the positions of hydration water molecules identified (see also panel B). The bar in the right side corresponds to 50 Å. The same coloring-scheme for the subunits is used for all the figures. (B) A stereoplot showing the distribution of hydration water molecules around subunit 1. The hydration water molecules interacting directly with only subunit 1 are presented as small red spheres. The orange fishnets superimposed on the ribbon model are omit-annealed difference electron density maps of hydration water molecules calculated with the reflections between the Bragg spacings of 8.0 and 2.25 Å and contoured at the 4.0σ level. The residues forming the active site are shown by stick models.

scale and spectacular movements of domains between their unligated and ligated states (*11*−*13*). The movements are indispensable to the biological functions, such as substrate binding and catalysis. As observed in T4-lysozyme (*14*−*16*) and calmodulin (*17*), multidomain enzymes exhibit spontaneous domain movements in their unligated state, and crystallization of the enzyme sometimes traps the transient state of the movement. Cryogenic X-ray crystal structure analyses for such crystals provide the trapped transient hydration structures as well as the trapped conformational state in the domain movements.

In the present study, we selected hexameric glutamate dehydrogenase (GluDH)[1] as a research target. GluDH is a multidomain enzyme catalyzing the reaction from glutamate to 2-oxyoglutarate and ammonia in the presence of the cofactor NAD or NADH (*18*), and the hexameric form (Figure 1 A) of GluDH is the biologically functional unit in some organisms (*19*). The subunit of hexameric GluDH consists of two separate domains of M_rs 23K: the nucleotide binding domain (N-domain) and the core domain engaging in the hexamer formation (C-domain) (Figure 1B) (*20*, *21*). Between the two domains, the active-site cleft harbors, and the substrate-binding site is located at the depth of the cleft (Figure 1B). The N-domain is known to exhibit a large-scale movement between the unligated and ligated states (*20*, *21*). In addition, crystal structures of unligated GluDH from

[1] Abbreviations: GluDH, glutamate dehydrogenase, rms, root-mean square; Rg, radius of gyration; SAXS, small-angle X-ray scattering; *Tp*, *Thermococcus profundus*; *Pf*, *Pyrococcus furiosus*; *Tm*, *Thermotoga maritima*; *Tl*, *Thermococcus litoralis*; *Cs*, *Clostridium symbiosum*.

various organisms and mutants exhibited variety in the orientations of the two domains (*20*, *22*−*29*), indicating spontaneous motion of the N-domain in solution like T4-lysozyme (*16*) and calmodulin (*17*). Mutational studies also supported the spontaneous fluctuation of the N-domain in the unligated state (*29*). However, no direct structural evidence has been reported for GluDH. In addition, as well as other multidomain enzymes, it is unknown what causes the domain motion and how the motion couples with the hydration water molecules surrounding the enzyme.

In the present study, the crystal structure of hexameric GluDH from hyperthermophile *Thermococcus profundus* (*30*, *31*) was determined at 110 K, including the large number of hydration water molecules. The motions of the N-domains in the six subunits were trapped differently in the crystallization process, and the hydration structures exhibited significant variations, in particular, in the active-site cleft. In addition, small-angle X-ray scattering (SAXS) profiles indicated the motion of the N-domain to be of larger magnitude in solution than in the crystalline state. Here we report the structural changes in both the enzyme and the hydration and discuss the possibility that a few hydration water molecules in the active site directly couple with the domain motion. The present report is the first to reveal that the hydration structures exhibit cooperative variation with the large-scale dynamical motion of enzymes at high resolution.

MATERIALS AND METHODS

Crystal Structure Determination. The purification and crystallization of recombinant GluDH of *Tp* were carried out as described previously (*31*, *32*). The crystals obtained belonged to space group $P2_1$ with the lattice constants of $a = 112.99$, $b = 163.70$, $c = 133.07$ Å, and $\beta = 113.46°$ at 110 K, and one hexamer of GluDH occupied a crystallographic asymmetric unit.

The diffraction intensity data were collected by the oscillation method at the BL44B2 beamline (*33*) of SPring-8 as previously reported (*32*). The programs DENZO and SCALEPACK (*34*) were used to process the diffraction intensity data (Table 1). The reflections were collected up to the resolution of 2.0 Å, and those up to 2.25 Å were used in the subsequent analysis, because the R^{I}_{merge} value was higher than 0.30 and the I/σ value lower than 3.0 beyond the Bragg spacing of 2.25 Å (Table 1).

The crystal structure of the GluDH hexamer was solved by the molecular replacement method using X-PLOR (*35*). The search model used for the analysis was constructed from the structural model of GluDH of *Pyrococcus furiosus* (*Pf*) (*22*) [the accession code is 1GTM in the Protein Data Bank (*36*)]. Through the rotation search followed by the Patterson-correlation refinement (*37*) and the subsequent translation search, one prominent solution was found. However, the structural models of the N-domains in subunits 1, 2, and 5 did not match with the calculated electron density maps, suggesting different quaternary structures in those subunits with the other. A rigid body refinement corrected the position of the N-domains and gave a nice match between the models and the calculated electron density maps. Because of this variation, we did not apply the noncrystallographic 32-symmetry constraint to the hexamer in the following structure refinement.

Table 1: Statistics of the Diffraction Data and the Refined Structural Model

data collection	
resolution (Å)	100.0−2.25
no. of observed reflections	1 488 939
no. of unique reflections	206 382
completeness (%)	99.7 (99.4)[a]
I/σ	17.9 (3.4)[a]
R^{I}_{merge} [b]	0.063 (0.322)[a]
refinement	
resolution (Å)	8.0−2.25
unique reflections ($F > 2\sigma$)	183 797
R-factor[c]	0.188
R-free[d]	0.250
structure model	
protein (non-hydrogen atoms)	19 250
sulfate ions	16
hydration water molecules	1931
bonds (Å)[e]	0.011
angle (deg)[e]	1.64
ion pair statistics[f]	
no. of ion pairs per hexamer	222
no. of ion pairs per residue	0.09
% of charged residues forming ion pairs	47
% of ion pairs formed by Arg/Lys/His	74/26/0
% of ion pairs formed by Glu/Asp	48/52

[a] The highest resolution shell is from 2.33 to 2.25 Å. [b] $R^{I}_{merge} = \sum_h\sum_i|I_i(h) - \langle I(h)\rangle|/\sum_h\sum_i I_i(h)$, where $I_i(h)$ is the intensity of ith observation of reflection h. [c] $R = \sum_h|F_{obs}(h) - F_{calc}(h)|/\sum_h F_{obs}(h)$, where $F_{obs}(h)$ and $F_{calc}(h)$ are the observed and calculated structure factors of reflection h, respectively. [d] R-free factor was calculated for 10% of unique reflections, which were not used in the structure refinement throughout (*45*). [e] Root-mean-square deviation from ideal stereochemical geometry. [f] The ion pair statistics were calculated by using the criteria of Barlow and Thornton (*46*). After the calculation, the geometry of the ion pairs was reexamined manually.

The structure refinement and model building were carried out with X-PLOR (*35*) and turbo FRODO (Biographics), respectively. The conventional protocol, including the simulated annealing, was applied under the stereochemical parameters proposed by Engh and Huber (*38*). The suit of program FESTKOP (*9*) carried out the picking-up of hydration water molecules from difference Fourier electron density maps. The hydration water molecules included in the model had thermal factors of less than 70 Å^2 and exhibited electron density peaks of more than 3.5σ in their omit-annealed difference Fourier electron density maps throughout the subsequent refinement rounds. The final statistics of the refined hexamer model were summarized in Table 1. The program DynDom (*12*) was used for analyzing the domain movement. The FESTKOP program (*9*) was used for systematically analyzing the first hydration shell. In the present study, the lower and the upper limits of the hydrogen bond distance were set at 2.4 and 3.4 Å, respectively.

Small-Angle X-ray Scattering Experiment. A small-angle X-ray scattering experiment was performed at BL45SX (*39*) of SPring-8. The X-ray wavelength was tuned to 1.0000 Å and the camera distance was set at 2200 mm. The CCD detector combined with an image intensifier (*40*) was used for recording the scattering pattern, and the exposure time was 1 s for each measurement. The circular averaging procedure (*40*) reduced the two-dimensionally recorded SAXS profiles.

The scattering experiments were carried out both at 293 and 338 K using a temperature controlled sample cell holder. Scattering profiles of sample solutions and buffers were

alternately measured to avoid systematic errors in the data analysis. To correct the concentration effect in the SAXS profile, the concentration of the enzyme solution was varied from 1.0 to 3.0 mg/mL in increments of 0.5 mg/mL. The concentration effect and the radius of gyration (Rg) were analyzed by using the suite of programs, iisgnapr (*40*). The pair-distribution function $P(r)$ was calculated by using the program GNOM (*41*). The program DEBYE (Nakasako, unpublished work) was used for the theoretical calculation of the scattering curve, the $P(r)$ function and the Rg value of the crystal structure.

RESULTS

Variety in the Quaternary Structures between the Six Subunits. Figure 1A shows the overall structure of the GluDH hexamer with 1931 hydration water molecules. The ion-pair statistics of the present structural model were very similar to those for GluDH from *Thermotoga maritima* (*Tm*) (*24*), and the thermostability of this enzyme will be discussed elsewhere. In the crystal lattice, the hexamers interact with adjacent ones through only 14 hydrogen bonds (<3.4 Å) and 19 van der Waals contacts (<3.7 Å). While the interactions are formed at the tips of N-domains in subunits 1, 2, 3, 4, and 5, the N-domain of subunit 6 is completely free from crystal contacts. The crystals analyzed here have appeared merely even through very careful preparation of the crystallization buffers (*32*). The small number of interactions in the crystal lattice may explain why the reproducibility of the crystallization is very low.

The six subunits appear in the different quaternary structures from each other with respect to the positions and orientations of N-domains relative to C-domains (Figure 2 A). Despite the variation, the structures of individual domains are nearly the same as indicated by the small positional differences of main chain atoms, less than 0.5 Å, between the subunits (Figure 2B). Analysis revealed the presence of a hinge, which rotates the N-domain more than 7° and shifts the tips of the N-domain more than 10 Å between subunit 1 and subunit 5 (Figure 2, panels A and B). The candidates for the residues forming the hinge are Gly182, Gly183, Leu185, and Gly186 nearby the active site and Gly361 far from the site (Figure 2A). These five residues compose two long loops connecting the two domains and are almost free from strong interactions with the other portions of the subunits. In particular, the variation of the ψ angle in Leu185 between 134 and 162° explains approximately the observed quaternary structures. As a result, the quaternary structures of the subunits are classified roughly into three with respect to the orientations of the two domains (Figure 2, panels A and B): subunit 1 is in the "open", subunits 2 and 5 in the "closed", and subunits 3, 4, and 6 in the "medium" state (Figure 2A). In addition, the ion pair networks in this hyperthermostable enzyme contribute little to restricting the domain motion (data not shown).

The variations in the quaternary structures are likely explained by the ideas that each subunit undergoes spontaneous hinge bending motion and that the motion is trapped in the intermediate state through the different modes of crystal contacts. The extremely large temperature factors in the N-domain of subunit 6 may support this idea. The factors in the domain of subunit 6 are more than twice those in the other subunits and are prominent at the tips of the N-domain. Because the N-domain of subunit 6 is completely free from crystal contacts, the temperature factors of its N-domains seem to reflect directly the fluctuating nature of the N-domain in solution.

Referring to the structure of the ligated enzyme from *Clostridium symbiosum* (*Cs*) (*21*), we identified the residues forming the active site (Figures 1B, 2A, and 3). Lys69, Met90, Asp145, and Thr175 are in nearly the same conformation in all the six subunits. Val348 and Ser351 belonging to the helix forming the bottom of the cleft exhibit small positional shifts of ∼1 Å through the displacement of the helix. The conformations of the side chains in Val348s are very similar of those observed in the ligated enzyme in *Cs* (*21*). In contrast, those of Ser351s are the same as in the unligated one (*20*). Therefore, The structural changes in the active-site cleft are small.

Hydration Structure Changes in the Active-Site Clefts of the Six Subunits. In the present study, the cryogenic X-ray diffraction experiment revealed numerous hydration water molecules to discuss the variation in hydration structure between the subunits. Except for subunit 6 with the N-domain exhibiting large positional fluctuation, around every subunit, 200−300 hydration water molecules in the first hydration shell were identified. The amounts correspond to 25−45% of the molecules required for the monolayer hydration of each subunit, when applying the average value of surface area covered by one water molecule in the first hydration shell (*9*). About 50% of hydration water molecules in the first hydration shell reside in nearly the same hydration sites in all subunits, and the rest exhibit positional differences of more than 1.3 Å.

The variety among hydration structures is most prominent in the active-site clefts, despite the small structural changes in the residues forming the cleft. Because the interior of the cleft is completely free from crystal contacts, the observed hydration structures in the clefts must reflect intrinsic forms during domain movement in solution. Therefore, a detailed comparison of the hydration structures between the three states may provide clues for discussing the mechanism in the reorganization of hydration structures coupling with the large-scale motion of the N-domain.

In the open state (subunit 1), 36 hydration water molecules adsorb densely in regions A, C, N, P, and R (Figure 3 A) of the cleft having dimensions of ∼16 Å wide and ∼12 Å deep. Three molecules are confined in sites B1−B3 of the relatively hydrophobic moiety inside the molecular surface of the enzyme. The molecules in region P are in a characteristic arrangement like a prop between the two domains. In addition, one sulfate ion occupies the substrate-binding site so that its two oxygen atoms take place the position of the substrate carboxyl group expected in the ligated *Cs* GluDH (*21*). This ion forms hydrogen bonds with the two hydration water molecules, B2 and P6, and a weak one with Lys 69. The middle of the cleft is free from hydration water molecules, indicating the inherent disorder of hydration structures in that space. The hydration water molecule A1 resides at nearly the same position as "Water 1", which has been found in *Cs* GluDH in the ligated state and is important for the hydride transfer reaction (*21*).

In the medium state (subunits 3, 4, and 6), the N-domain shifts toward the C-domain by ∼2 Å at the mouth and ∼0.5

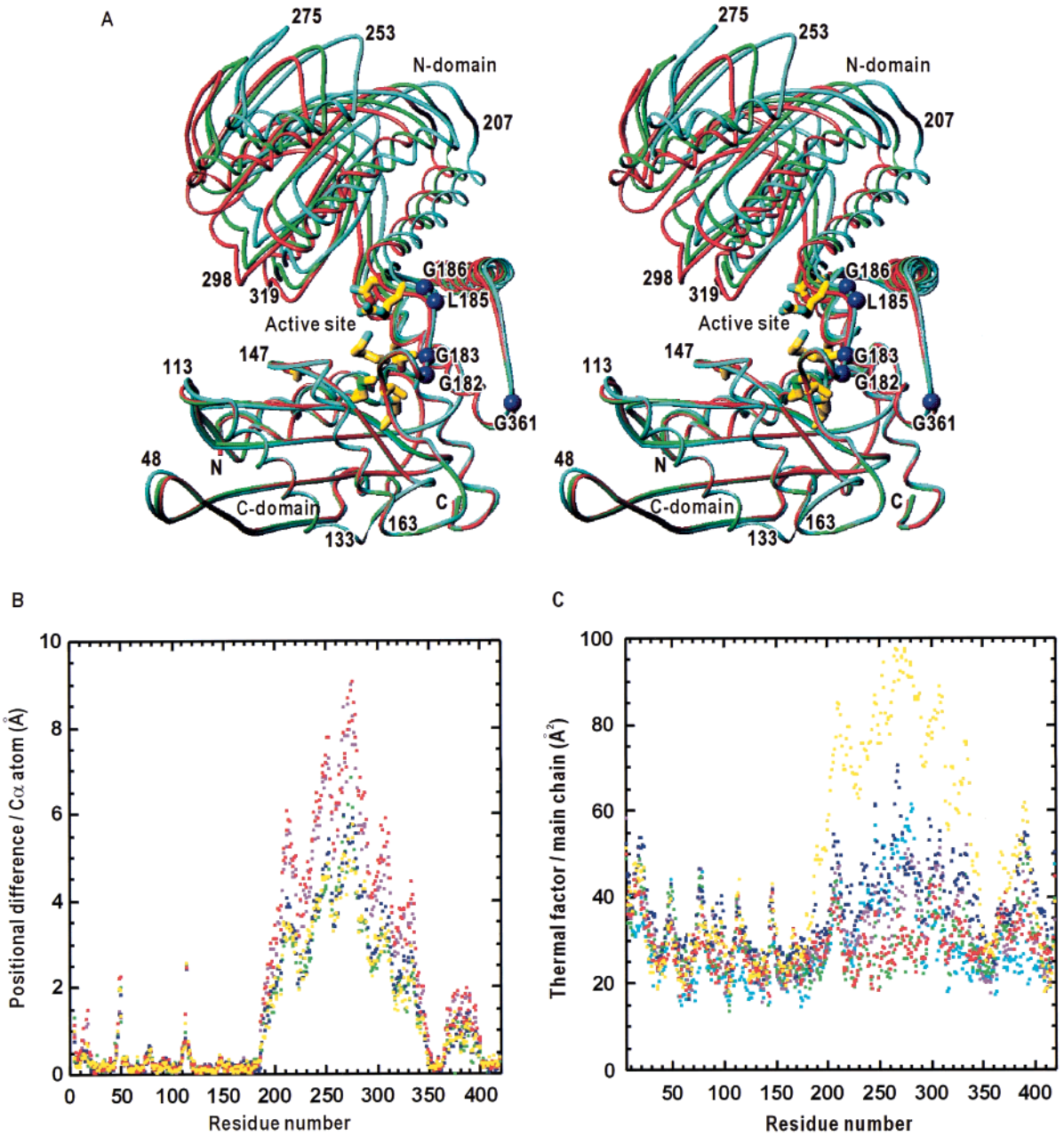

FIGURE 2: (A) stereoplot for the Cα-traces of subunits 1 (cyan), 3 (green), and 5 (red) after overlapping optimally their main chain atoms in the C-domains. The blue spheres indicate the positions of the residues composing the hinge (see test). The colored stick models are the side chains of the residues forming the active site in subunit 1. (B) The positional differences of Cα atoms in subunits 2−6 from those in subunit 1 are plotted against the residue number. The difference values are calculated after optimally superimposing the C-domain of each subunit onto the domain in subunit1 as shown in panel A. For the C-domains, the overall rms difference values between the Cα atoms of six subunits ranged from 0.17 to 0.45 Å. (C) The average thermal factors of main chain atoms of six subunits plotted against the residue number. The colors of the dots in panels B and C are in accordance with the coloring scheme of subunits defined in Figure 1A.

Å at the depth of the cleft relative to the open state (Figure 3B). Some hydration water molecules identified in regions A and N of the open state (Figure 3A) are inappreciable in the electron density maps of the three subunits in the medium state, and the molecules at sites B1−B3 in the open state completely disappear. As a result, the number of hydration water molecules is the smallest among the three state as an average (23 molecules in subunit 3, 19 in subunit 4, and 21 in subunit 6). In addition, the hydration water molecule A0 takes the place of the sulfate ion found in the open state. The prop-like arrangement in region P is broken at the middle (P3 and P4), and the three hydration water molecules in the upper part (P1−P3) shift together toward the C-domain by 1.4 Å. Between the two domains, hydration water molecules R2−R5 appear around the mouth of the cleft so as to extend the network of hydrogen bonds in front of Arg187.

Further closing of the N-domain narrows the cleft by ∼2 Å at the mouth and ∼0.5 Å at the depth. In the closed state (Figure 2A), the number of identified hydration water molecules is 27 and 30 in subunits 2 and 5, respectively. The increase in the amount of hydration water molecules in regions A and N in the closed state contrasts with the decrease in the medium state described above. The molecule A0 at the depths still resides at the binding site of the sulfate

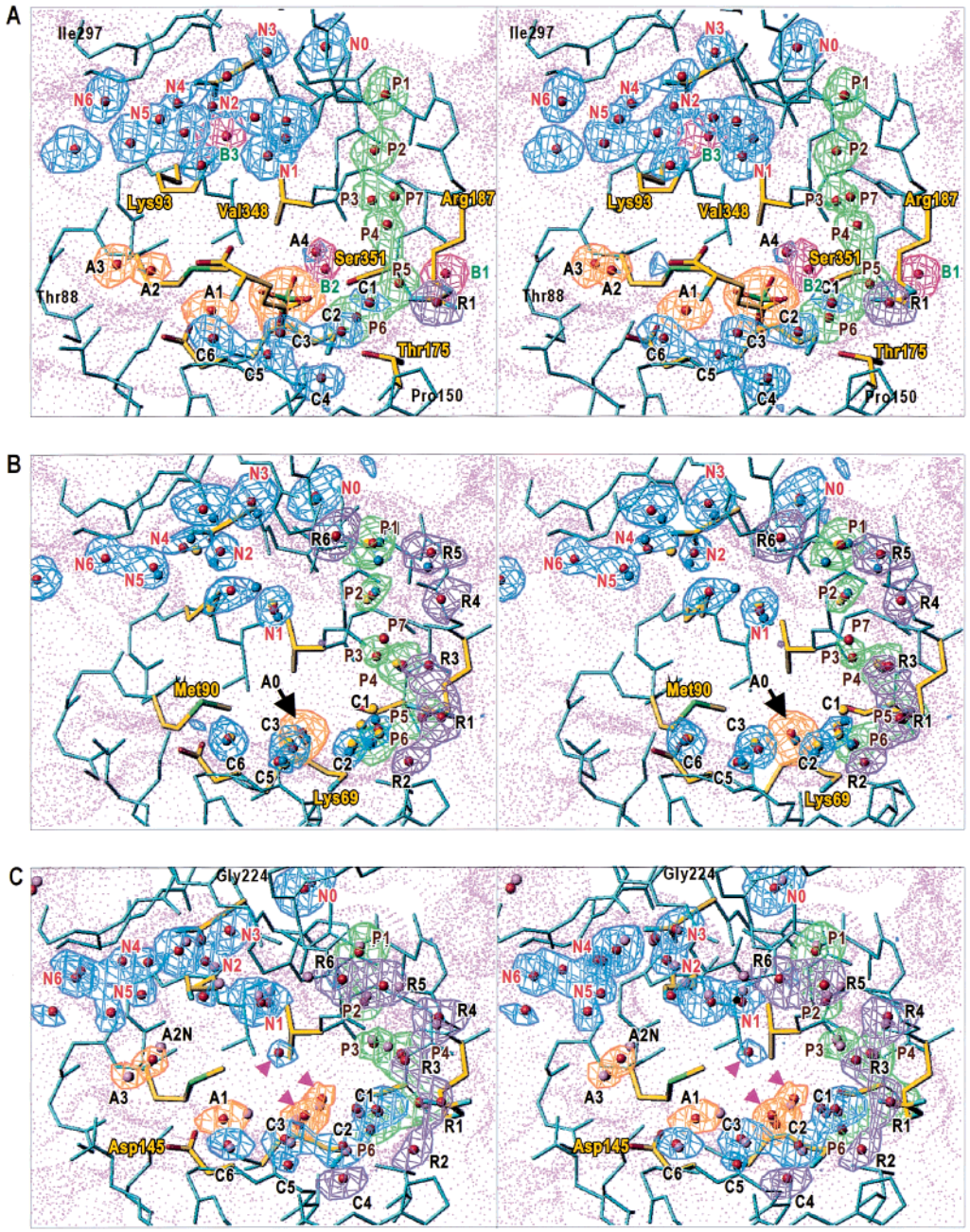

FIGURE 3: Stereoplots of the hydration structures in the active-site cleft in subunit1 (A), subunit 3 (B), and subunit 5 (C). The main chain and some side chains of the subunits are presented as cyan-colored stick models. The bold stick models show the residues forming the active site. The colored spheres indicate the positions of hydration water molecules. The red spheres in panels A, B, and C are the positions of the molecules in subunits 1, 3, and 5, respectively. In panel B, the blue spheres are those of subunit 4, and the yellow ones are of subunit 6. In panel C, the purple spheres are of subunit 2. The omit-annealed difference electron density maps of the solvent molecules are superimposed in the same way as in Figure 1B. For clarity, the colors of the maps are distinguished depending on the location of the hydration water molecules. The hydration water molecules are named and numbered as follows: the molecules adsorbing on the floor of C-domain are labeled as "C", below N-domain as "N", around Arg187 as "P" and "R", around the substrate binding site as "A" and in the hydrophobic cavities behind the molecular surface as "B". The dots in pink represent the molecular surface around the active sites calculated by Connolly's method (*48*) with a probe radius of 1.4 Å.

ion, and three molecules surrounding it (indicated by red arrows in Figure 3C) are located at suitable positions for hydrogen bonding with the molecules P6 and N1. The other three molecules near Met 90 and Asp 145 reside at sites nearly identical with those in the open state. On the surface of the N-domain, the population of hydration water molecules more closely resembles that in the open state rather than the medium states with respect to both the arrangement and the amount.

The domain motion presumably causes these changes in hydration structure in the cleft. In particular, the hydration structure changes in regions B, P, and A are very interesting when examining the dynamical coupling between the domain motion and reorganization in hydration structure in this enzyme.

Hydration Structure around the Hinge Region. The positional shifts of the residues in the hinge regions are ~1.5 Å between the open and the closed state (Figure 2B). The

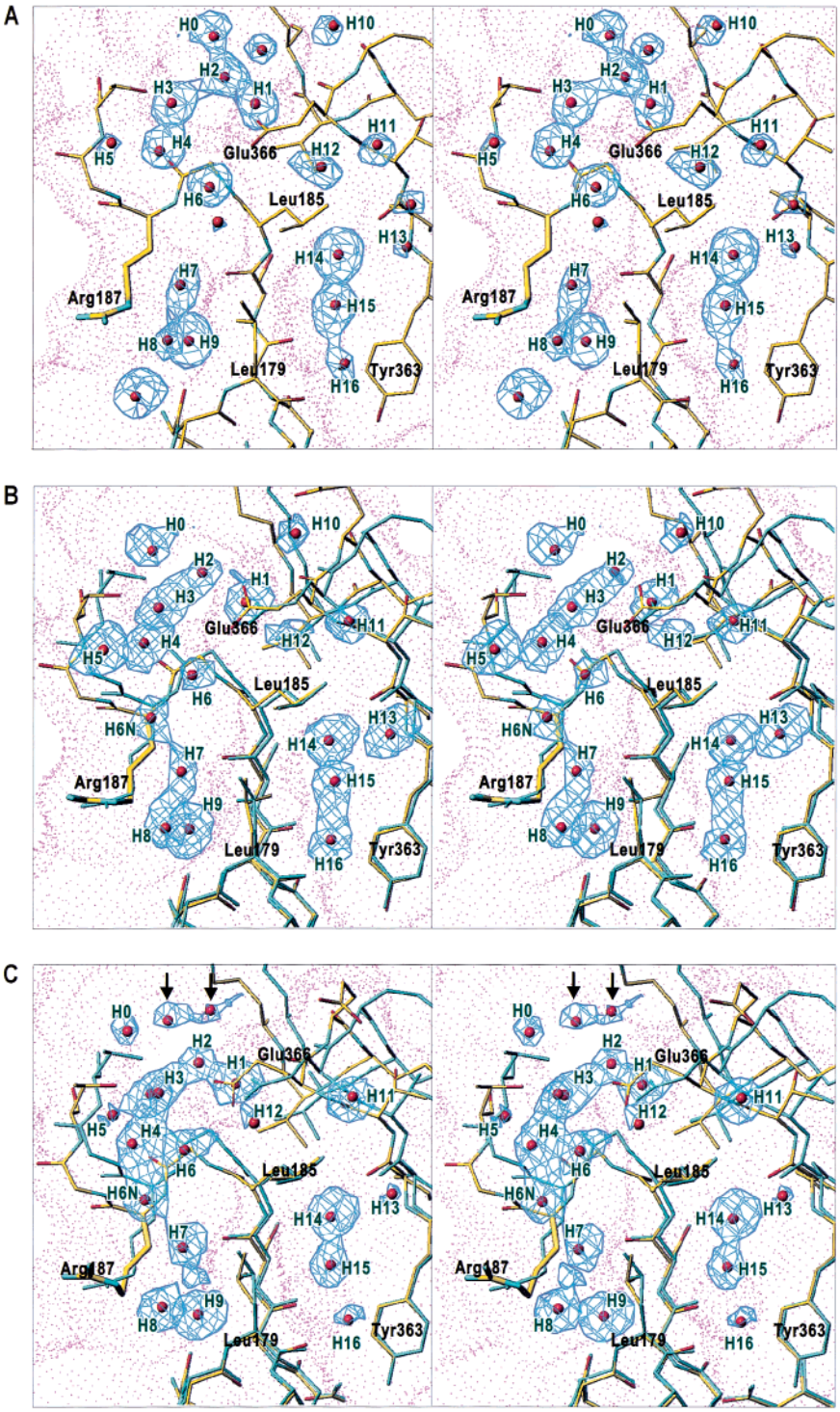

FIGURE 4: Stereoplots of the hydration structures around hinge regions of subunit 1 (A), subunit 3 (B), and subunit 5 (C). The red spheres show the positions of hydration water molecules, and the blue fishnets are the omit-annealed difference electron density maps calculated and contoured in the same way as in Figure 1B. In panels B and C, the structural models of subunit 1 (colored in cyan) are superposed after overlapping the C-domains to show clearly the structural changes in the hinge regions between the subunits. Hydration water molecules appearing in at least two subunits are numbered H1−H16. The small dots represent the molecular surface around the hinge regions. Some residue numbers are inserted. The pink dots are the molecular surface as in Figure 3.

shifts are comparable in magnitude to those in the active-site clefts; however, the hydration structures are invariant in contrast with the active site (Figure 4).

In the open state (subunit 1), 18 hydration water molecules cover the hinge region (Figure 4A). Most of these (H0−H4, H6−H9, and H14−H16) reside in the grooves on the surface, while the four molecules, H10−H13, contribute to the hydrophobic hydration of Leu185. In the closing motion of the N-domain, almost all of the hydration water molecules move together with the N-domains (Figure 4, panels B and C). In the closed state, the hydration water molecules indicated by arrows in Figure 4C newly appear and likely contribute to the stabilization of the hydration structure and the extension of the network around Glu366.

Little change in the hydration structure around the hinge implies that the structural changes around the hinge are

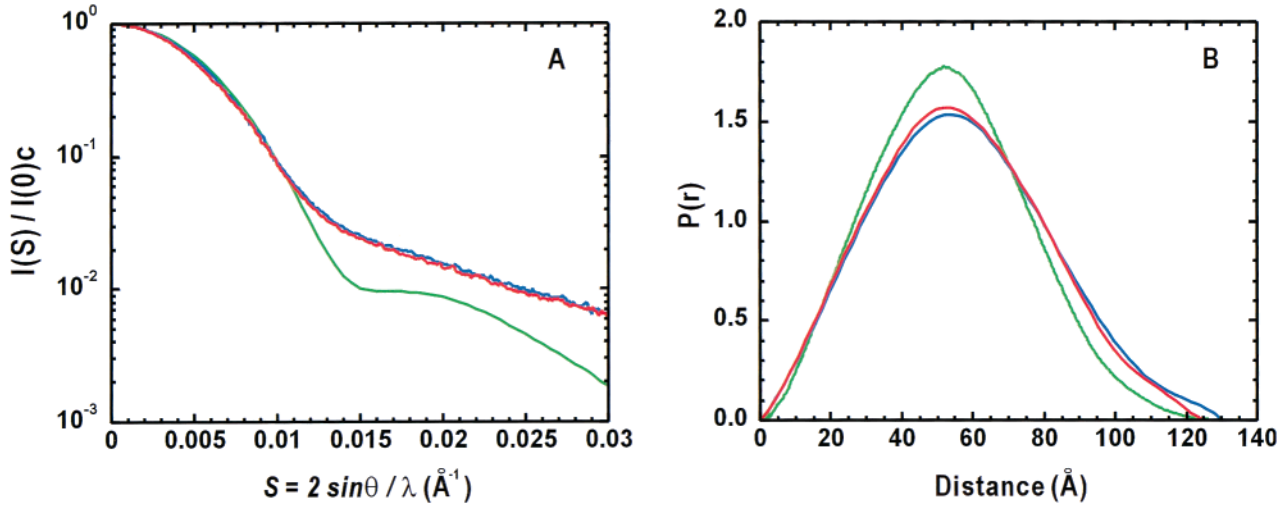

FIGURE 5: (A) Comparison of the small-angle X-ray scattering profiles of GluDH measured at 293 K (blue dots) and 338 K (red dots) with that calculated from the crystal structure (green line). The experimental curves are obtained after correcting for the concentration effects. All scattering curves are normalized so that the zero-angle scattering intensity is equal to 1.0. (B) The pair-correlation functions [$P(r)$] calculated from the measured scattering curves at 293 K (blue dots), at 338 K (red dots) and directly calculated from the crystal structure (green line). All $P(r)$ functions are normalized so that the integration of each function up to the maximum correlation distance gives unity.

approximated as a rigid body motion keeping the hydration sites. The flexible hinge may be forced to rotate by a structural change occurring in the other portion of the subunit, presumably in the active site as discussed below.

Small-Angle X-ray Scattering Profiles of GluDH in Solution. One question arises as to the structure of *Tp* GluDH: is the quaternary structure in solution at the near physiological temperature of the enzyme (338 K) the same as that determined in the crystalline state at 110 K? Figure 5 shows the results from the SAXS experiments for GluDH hexamer in solution both at 293 and 338 K. All profiles in the very small angle region ($S < 0.007$ Å^{-1}) are well approximated by Guinier's formula (*42*). The radius of gyrations (Rgs) of the hexamers were determined to be 43.92 (± 0.03) Å at 293 K and 43.05 (± 0.05) Å at 338 K after correcting for the concentration effect (*42*). The SAXS profiles had a characteristic bend at $S \approx 0.015$ Å^{-1} (Figure 5A). The pair-correlation functions, i.e., $P(r)$ functions, have unimodal shapes with maximum dimensions of 127−130 Å (Figure 5B). The coincidence of the profiles and the functions between the two temperatures indicate that the overall structure of *Tp* GluDH is independent of temperature between 293 and 338 K, when viewed at such a low resolution.

The scattering profile and the $P(r)$ function calculated from the crystal structure show substantial differences from those observed (Figure 5). The calculated profile has a broad peak at around 0.02 Å^{-1} originating from the cylindrical shape of the hexamer (a diameter of 100 Å and height of 100 Å). The calculated Rg (40 Å) is smaller than those observed, even when all hydration water molecules identified were included in the calculation (Rg = 41 Å). In addition, the calculated $P(r)$ function has a maximum correlation length of 110 Å, and its profile deviates from the observed ones beyond 60 Å. These discrepancies imply that the apparent molecular shape of the hexamer deviates from the crystal structure and that the apparent molecular size of the hexamer is slightly larger in solution than in the crystalline state. The central portion of the hexamer is composed of six C-domains assembled through a large number of strong hydrogen bonds and van der Waals interactions. In addition, the structures of individual domains act as rigid bodies as shown in Figure 2A. Thus, the dynamical movement of N-domains in solution should be responsible for the discrepancies in both the SAXS profiles and the $P(r)$ functions.

DISCUSSION

The six subunits in the crystal structure of the unligated hexameric GluDH from *Tp* display roughly three quaternary structures with respect to the positions and the orientations of the cofactor-binding domains relative to the hexamer-forming domains. The SAXS profiles of the hexamer coincide well at 293 and 338 K, but have substantial differences with that calculated from the crystal structure. The hydration structures in the active-site cleft vary markedly with the domain motion. Here we discuss the spontaneous domain motion in *Tp* GluDH and the implications of the hydration structure changes for the dynamics and the function of this enzyme.

Spontaneous Domain Motion of Tp GluDH. The present crystal structure analysis has provided evidence of spontaneous domain motion of *Tp* GluDH in solution. (i) The variations in the quaternary structures of the six subunits are explained by a hinge bending motion (Figure 2, panels A and B). (ii) The flexible hinges are free from the structural rigidity of subunits originating from the ion pair networks stabilizing the structure of the enzyme. (iii) The exceptionally large temperature factors in the N-domain of subunit 6 reflect directly the mobility of the domain (Figure 2C). These structural findings indicate that the N-domain undergoes large-scale spontaneous motion in solution and that the metastable intermediates in the motion are trapped in the structures observed in the crystal.

To explain the discrepancies in the SAXS profiles and the $P(r)$ functions shown in Figure 5, we made various types of hexamer models with respect to the position and orientation of the N-domains. However, none could explain the discrepancies, indicating that the observed profile is an ensemble of hexamers in different quaternary structures. The enzyme in the unligated form is in a state of spontaneous domain

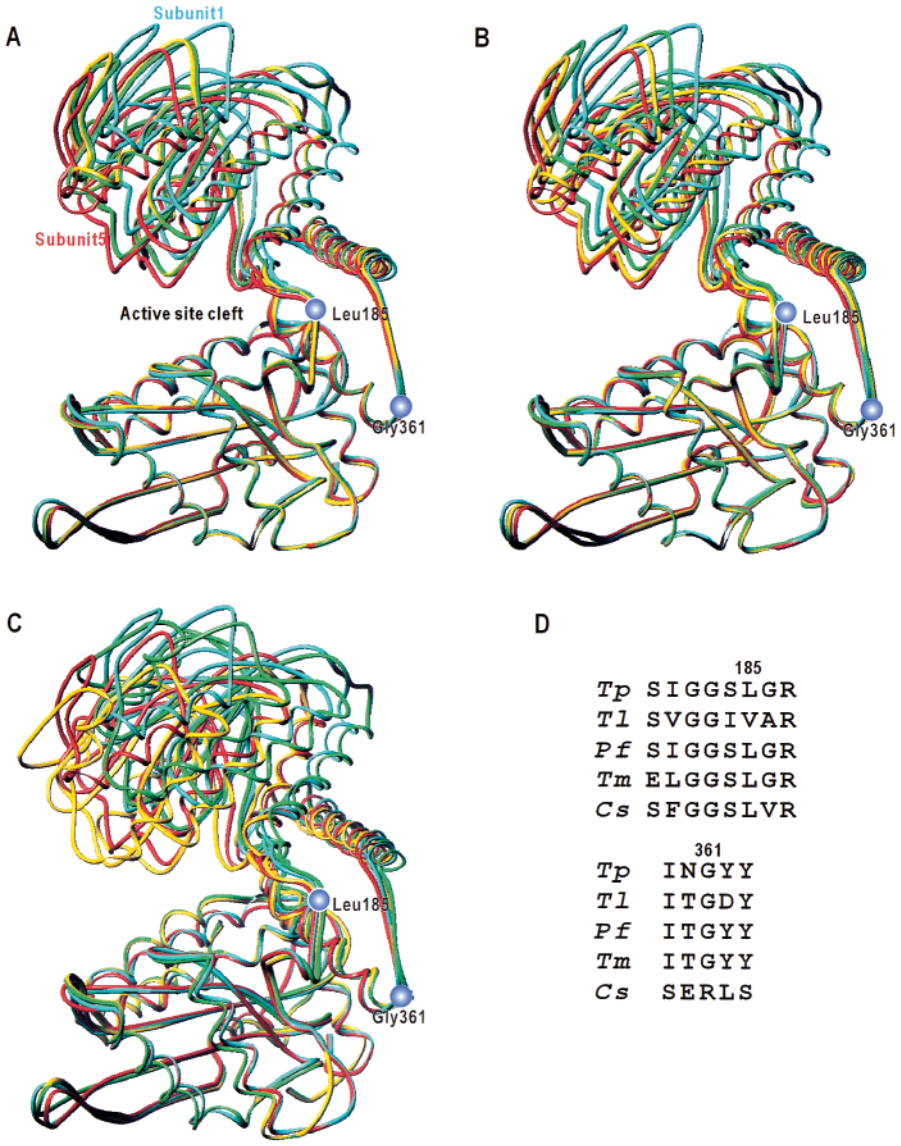

FIGURE 6: Comparison of the quaternary structures of subunits in GluDHs from various organisms. Throughout the figures, simultaneously superimposed are subunits 1 (cyan-colored model) and 5 (red) of *Tp*. (A) A plot superimposing subunit 1 (colored in green) and subunit 2 (yellow) of *Pf* GluDH (the accession code in the Protein Data Bank is 1GTM) (*22*). The structures of subunits in GluDH from *Tm* [1B26 (*24*) and 1B3B (*25*)] are in the nearly the same conformation with that of subunit 1 from *Pf*. (B) A plot for subunit 4 (yellow) and 5 (green) in *Tl* GluDH [1BVU (*26*)]. The N-domains of the two subunits are the extreme positions in the six subunits. Subunits 3 and 6 of mutant GluDH from *Tm* [2TMG (*27*)] exhibit similar variations with those of *Tl*. (C) Superimposed are subunit 3 (green) [the most open conformation in the model 1HRD (*20*)] of unligated *Cs* GluDH and a subunit of the ligated state of the enzyme (yellow) [1BGV (*21*)]. (D) Alignments of amino acid sequences around the hinge region of GluDHs from *Tp*, *Tl*, *Pf*, *Tm*, and *Cs*.

motion in solution through various conformational state. The results and ideas presented here are consistent with the proposal from mutational studies on *Cs* GluDH (*21*). The small structural changes in Leu185 and the involvement of several glycine residues in the hinge region (Figure 2A) ensure the domain motion without loss or gain of a large amount of internal free energy of the enzyme.

The observed quaternary structures are similar to the crystal structures of GluDHs from other organisms (Figure 6). For instance, the orientation of the two domains in the medium state is very similar to that of hyperthermostable GluDHs from *Pf* (*22*), *Tm* (*24*), or *Thermococcus litralis* (*Tl*)- (except for subunit 4 of that enzyme) (*26*) (Figure 6, panels A and B). Some structural characteristics of the closed state are seen in ligated GluDH from *Cs* (*21*), and the structure of the open state is comparable with subunit 2 of unligated GluDH from *Cs* (*20*) (Figure 6C). Among the hyperthermostable GluDHs, identity in amino acid sequence is very high, and the sequence in the hinge region is well conserved (Figure 6D). Therefore, the variations in the quaternary structures of GluDHs from various organisms are likely explained by the N-domain motion of GluDH in the unligated state and not by the idea that the variations are artifacts caused by the crystallization conditions.

Spontaneous domain motions of enzyme have been reported in T4 lysozyme (*14*−*16*) and calmodulin (*17*). The crystal structures of the enzymes are explained as conformational substates trapped through different modes of crystal packing (*15*). A detailed study on the crystal structure of bovine pancreatic trypsin inhibitors has suggested that the conformations observed are intrinsic sub-states of the protein (*43*). The roughly three domain orientations in *Tp* GluDH and the other GluDHs must be conformational substates of the domain motion in the unligated state.

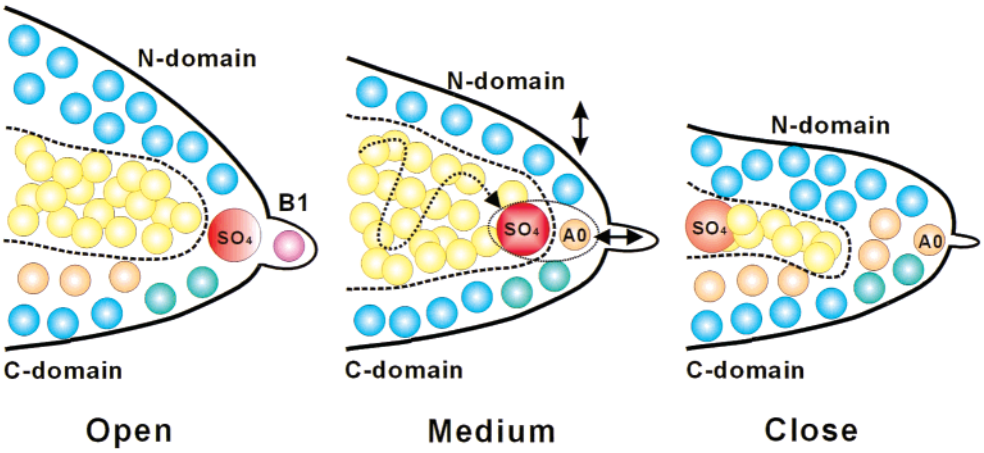

FIGURE 7: Schematic illustration of the proposed scheme for sulfate ion binding. Ordered hydration water molecules are presented by cyan, orange, green, and pink colored spheres in the same coloring scheme used in Figure 3, and disordered ones, which are missed in the experimental electron density maps, in yellow. The dashed lines indicate a schematic border between the ordered and disordered hydration structures. The dotted line schematically illustrates the wandering of the sulfate ion in the active-site cleft.

Hydration Structure Changes in Coupling with the Domain Motion. While the amount of hydration water molecules is still less than half of that required for the monolayer hydration, the present crystal structure provides novel structural information on hydration in the active-site cleft during the domain motion (Figure 3). Here, we discuss the correlation between the spontaneous large-scale domain motion and the hydration structures to understand why the domain motion occurs spontaneously.

Of the observed variations in hydration structure in the active-site cleft, changes in B and P sites seem to be of particular importance to the coupling between the hydration structures and the spontaneous domain movement between the open and medium state (Figure 3, panels A and B). The six hydration water molecules in B1−B3 and P1−P3 in the open state must disturb the closure movement of the N-domain and simultaneously contribute to stabilizing the open state. Therefore, from the open toward the medium state, the molecules at B sites must be squeezed out or spontaneously escape in coupling with the N-domain movement narrowing the dimensions of the sites (for example, migrations between B1 and P5, B2 and A0, and B3 and N1 presumably occur) (Figure 3, panels A and B). In a similar way, P1−P3 molecules shift together.

In molecular dynamics simulation of water, water molecules exhibit intermittent hopping in their migration reorganizing the networks of hydrogen bonds (*44*). If the hydration water molecules at B sites retain this property, they will hop between B sites and the other sites in the clefts. Therefore, the domain movements between the open and the medium states may occur as a stepwise process through the limited number of conformational sub-state specified by the cooperative dissociation/association and hopping migration of the hydration water molecules at sites B and P.

As described in the previous section, the structures and interactions of the hinge ensure spontaneous N-domain motion of *Tp* GluDH. Therefore, the inherent mobility of hydration water molecules, in particular in the active-site cleft, and the intrinsic fluctuating nature of the hinge regions may together cause the domain motion.

Hypothetical Scheme on the Hydration-Coupled Substrate Binding. The variation of hydration structures in region A implies a hypothetical but attractive scheme for the binding of sulfate ion or substrate to GluDH (Figure 7). Both in the medium and the closed state, sulfate ions are absent from the binding site, although the dimensions of the cleft alone are large enough for sulfate ion to access the depth (Figure 3, panels B and C). In the closed state, the network of hydration structures in region A prevents the intrusion of ion (Figure 3C). In the medium state, sulfate ions may be forced to wander in the cleft because of the disordered hydration structures (Figures 3B and 7). However, wandering ions occasionally form hydrogen bonds with a hydration water molecule at site A0 (Figure 3B). At that time, when the molecule at A0 migrates to site B2 in coupling with the N-domain movement opening the cleft, the ion is presumably pulled into the binding site A0 in keeping the hydrogen bonds (Figure 7). The ligated state of this enzyme may be realized in a similar way. The substrate forms extra hydrogen bonds with Asp 145 and Lys 93 (Figure 3A) (*21*). The residence of the substrate in the site is guaranteed by the interactions until the chemical reaction is finished after closing of the N-domain.

According to this idea, sulfate ions or substrates can access the active site only in a certain range of domain movement, in which hydration structures are suitable and assist the intrusion of them. Therefore, the domain movement likely hinders the smooth binding of sulfate ion or substrate to the active site. The N-domains undergo greater hinge motion in solution than in the crystal structure as indicated by the substantial differences between the SAXS profiles of GluDH in solution and that of the crystal structure (Figure 5). The occasion of ion or substrate binding to the site may be greater in solution than in crystalline state. However, many intermediate states in the domain motion, are still "idle" for realizing the substrate binding. The idling states slow the turnover rate of GluDH even at the "ambient temperature" of this hyper-thermostable enzyme. Indeed, the value for glutamate is 20 ms at 338 K (*30*).

REFERENCES

1. Eisenberg, D., and Kauzmann, W. (1969) *The structure and properties of Water*, Oxford at the Clarendon Press, London.
2. Levitt, M., and Park, B. H. (1993) *Structure 1*, 223−226.

3. Finner-Moore, J. S., Kossiakoff, A. A., Hurley, J. H., Earnest, T., and Stroud, R. M. (1992) *Proteins: Struct., Funct., Genet. 12*, 203−222.
4. Ferrand, M., Dianoux, A. J., Petry, W., and Zaccai, G. (1993) *Proc. Natl. Acad. Sci. U.S.A. 90*, 9668−9672.
5. Hayward, S., Kitao, A., Hirata, F., and Go, N. (1993) *J. Mol. Biol. 234*, 1207−1217.
6. Lounnas, V., and Pettit, M. (1994) *Proteins: Struct., Funct., Genet. 18*, 133−147.
7. Burling, F. T., Weis, W. I., Flaherty, K. M., and Brünger A. T. (1996) *Science 271*, 72−77.
8. Suzuki, M., Shigematsu, J., and Kodama, T. (1996) *J. Phys. Chem. 100*, 7279−7282.
9. Nakasako, M. (1999) *J. Mol. Biol. 289*, 547−564.
10. Nakasako, M., Takahashi, H., Shimba, N., Shimada, I., and Arata, Y. (1999) *J. Mol. Biol. 291*, 117−134.
11. Gerstein, M., Lesk, A. M., and Chothia, C. (1994) *Biochemistry 33*, 6739−6749.
12. Hayward, S., and Brendsen, H. J. C. (1998) *Proteins: Struct., Funct., Genet. 30*, 144−154.
13. Gerstein, M., and Krebs, W. (1998) *Nucleic Acids Res. 26*, 4280−4290.
14. Faber, H. R., and Matthews, B. W. (1990) *Nature 348*, 263−266.
15. Zhang, X. J., Wozniak, J. A., and Matthews, B. W. (1995) *J. Mol. Biol. 250*, 527−552.
16. Mchaourab, H. C., Oh, K. J., Fang, C. J., and Hubbell, W. L. (1997) *Biochemistry 36*, 307−316.
17. Zhang, M., Tanaka, T., and Ikura, M. (1995) *Nat. Struct. Biol. 2*, 758−767.
18. Frieden, C. (1963) in *The Enzymes* (Boyer, P. D., Ed.) Vol. 7, pp 3−24, Academic Press, New York.
19. Britton, K. L., Baker, P. J., Rice, D. W., and Stillman, T. J. (1992) *Eur. J. Biochem. 209*, 851−859.
20. Baker, P. J., Britton, K. L., Engel, P. C., Farrants, G. W., Lilley, K. S., Rice, D. W., and Stillman, T. J. (1992) *Proteins: Struct., Funct., Genet. 12*, 75−86.
21. Stillman, T. J., Baker, P. J., Britton, K. L., and Rice, D. W. (1993) *J. Mol. Biol. 234*, 1131−1139.
22. Yip, K. S. P., Stillman, T. J., Britton, K. L., Artymiuk, P. J., Baker, P. J., Sedelnikova, S. E., Engel., P. C., Pasquo, A., Chiaraluce, R., Consalvi, V., Scandurra, R., and Rice D. W. (1995) *Structure 3*, 1147−1158.
23. Baker, P. J., Waugh, M. L., Wang, X.-G., Stillman, T. J., Turnbull, A. P., Engel, P. C., and Rice, D. W. (1997) *Biochemistry 36*, 16109−16116.
24. Knapp, S., de Vos, W. M., Rice, D., and Ladenstein, R. (1997) *J. Mol. Biol. 267*, 916−932.
25. Lebbink, J. H., Knapp, S., van der Oost, J., Rice, D., Ladenstein, R., and de Vos, W. M. (1998) *J. Mol. Biol. 280*, 287−296.
26. Britton, K. L., Yip, K. S., Sedelnikova, S. E., Stillman, T. J., Adams, M. W., Ma, K., Maeder, D. L., Robb, F T., Tolliday, N., Vetriani, C., Rice, D. W., and Baker, P. J. (1999) *J. Mol. Biol. 293*, 1121−1132.
27. Lebbink, J. H., Knapp, S., van der Oost, J., Rice, D., Ladenstein, R., and de Vos, W. M. (1999) *J. Mol. Biol. 289*, 357−369.
28. Peterson, P. E., and Smith, T. J. (1999) *Structure 7*, 769−782.
29. Stillman, T. J., Migueis, A. M. B., Wang, X.-G., Baker, P. J., Britton, K. L., Engel, P. C., and Rice, D. W. (1999) *J. Mol. Biol. 285*, 875−885.
30. Kobayashi, T., Higuchi, S., Kimura, K., Kudo, T., and Horikoshi, K. (1995) *J. Biochem. (Tokyo) 118*, 587−592.
31. Higuchi, S., Kobayashi, T., Kimura, K., Horikoshi, K., and Kudo, T. (1997) *J. Ferment. Bioeng. 83*, 405−411.
32. Higuchi, S., Nakasako, M., and Kudo, T. (1999) *Acta Crystallogr., Sect D 55*, 1917−1919.
33. Adachi, S., Oguchi, T., and Ueki, T. (1996) *SPring-8 Annual Report 1996*, 239−240.
34. Otwinowski, Z., and Minor, W. (1997) *Methods Enzymol. 276*, pp 307−326.
35. Brünger, A. T. (1992) *X-PLOR Version 3.1: A system for X-ray crystallography and NMR*, Yale University Press, New Haven, CT.
36. Bernstein, F. C., Koetzle, T. F., Williams, G. J. B., Meyer, E. F., Brice, M. D., Rodgers, J. R., Jr., Kennard, O., Shimanouchi, O., and Tasumi, M. (1977) *J. Mol. Biol. 112*, 535−542.
37. Brünger, A. T. (1990) *Acta Crystallogr., Sect. A 46*, 46−57.
38. Engh, R. A., and Huber, R. (1991) *Acta Crystallogr., Sect A 47*, 392−400.
39. Fujisawa, T., Inoue, K., Oka, T., Iwamoto, H., Uruga, T., Kumasaka, T., Inoko, Y., Yagi, N., Yamamoto, M., and Ueki, T. (2000) *J. Appl. Crystallogr. 33*, 797−800.
40. Fujisawa, T., Inoko, Y., and Yagi, N. (1999) *J. Synchrotron Rad. 6*, 1106−1114.
41. Svergun, D. I. (1992). *J. Appl. Crystallogr. 25*, 495−503.
42. Glatter, O., and Kratky, O. (1982) *Small-Angle X-ray Scattering*, Academic Press, London.
43. Kossiakoff, A. A., Randal, M., Guenot, J., and Eigenbrot, C. (1992) *Proteins: Struct., Funct., Genet. 14*, 65−74.
44. Ohmine, I., and Tanaka, H. (1993) *Chem. Rev. 93*, 2545−2566.
45. Brünger, A. T. (1992) *Nature 355*, 472−475.
46. Barlow, D. J., and Thornton, J. M. (1983) *J. Mol. Biol. 168*, 867−885.
47. Kabsch, W., and Sander, C. (1983) *Biopolymers 22*, 2577−2637.
48. Connolley, M. L. (1983) *Science 221*, 709−713.

BI002482X